2009

Grain refinement in dual-phase steels

K. Mukherjee
University of British Columbia

Sujoy Hazra
University of Wollongong, ssh755@uow.edu.au

M. Militzer
University of British Columbia

Grain Refinement in Dual-Phase Steels

K. MUKHERJEE, S.S. HAZRA, and M. MILITZER

Deformation-induced ferrite transformation (DIFT) was applied in laboratory tests to produce fine-grained dual-phase (DP) steels. Four different chemistries were investigated, starting from a conventional DP 600 chemistry of 0.06 wt pct C-1.9 wt pct Mn-0.16 wt pct Mo and subsequently varying Nb and Mo additions. For all investigated steels, ultrafine ferrite (UFF) with a grain size of 1 to 2 μm can be obtained when a sufficient amount of deformation (*e.g.*, a true strain of 0.6 or above in axisymmetric compression) is applied to an austenite microstructure with a grain size in the range of 10 to 20 μm at 25 °C to 50 °C above the austenite-to-ferrite transformation start temperature (Ar_3) characteristic for the given cooling condition. Rapid post-deformation cooling at rates of approximately 100 °C/s yields the desired UFF-martensite microstructure. Electron backscattered diffraction (EBSD) mapping reveals a high percentage (approximately 40 pct) of low-angle boundaries in these microstructures, except for the steel that is just microalloyed with Nb. The steel with the plain-carbon-base chemistry was subjected to hot torsion simulations of a hot strip rolling processing schedules that incorporate a DIFT pass after a conventional seven-stand finish mill schedule. Executing the DIFT pass at 650 °C to 675 °C produced an UFF microstructure, illustrating the potential for the design of novel thermomechanical processing paths to produce hot-rolled ultrafine DP steels.

DOI: 10.1007/s11661-009-9899-9

I. INTRODUCTION

STEEL is widely used in the automotive and construction sector, due to its high strength and low cost. By enhancing the mechanical properties of steel, weight reduction in vehicles can be achieved and thinner cross sections of steel products can be used in the construction industries. Grain refinement increases the yield strength, which is the most important criterion for construction applications. For automotive applications, there are also other criteria to be considered, *e.g.*, initial work-hardening rate and uniform elongation. Grain refinement results in reduced uniform elongation and, hence, it makes steel unusable for those automotive parts for which high press formability is required. A combination of high strength, excellent elongation, and superior crashworthiness can be achieved by a variety of multiphase steels, *e.g.*, dual-phase (DP) and transformation-induced plasticity steels.[1] Aside from the multiphase concept, these steels benefit in general from a refinement of the microstructure. For fine-grained DP steels, this has recently been demonstrated by Park *et al.*[2] They obtained ultrafine-grained DP steel by equal-channel angular pressing and subsequent intercritical annealing. This steel displayed higher strength and total elongation than coarse-grained DP steel. It is interesting that the yield ratios and uniform elongations are comparable for both steels. However, because the volume fraction of martensite also increased in the case of the ultrafine-grained steel as compared to the coarse-grained steel, a detailed quantification of the effect of grain refinement on mechanical properties cannot be concluded from their study. Nevertheless, these results indicate the potential for improved mechanical properties by refined microstructures in DP steels and provide the incentive for investigating processing routes that are, in principle, suitable for producing fine-grained DP steel sheet.

Currently, asymmetric rolling, the deformation and annealing of martensite, the dynamic recrystallization of ferrite, and deformation-induced ferrite transformation (DIFT) are the most promising routes for obtaining ultrafine-grained steel sheets. Morimoto *et al.*[3] reported the industrial production of fine-grained steel at Nakayama Steel (Osaka, Japan) with a grain size of 2 to 5 μm in a 2-mm-thick plain-C steel strip by applying asymmetric rolling. Recently, Ueji *et al.*[4] and Tsuji *et al.*[5] have proposed a process route in which, starting with a martensite microstructure, a plain-C steel is cold rolled to a reduction of 50 pct and subsequently annealed at 500 °C to produce submicron-sized ferrite grains by recrystallizing martensite. Alternatively, Longfei *et al.*[6] achieved ferrite grain refinement in a low-carbon steel by deformation in the ferrite phase region. According to their investigation, the dynamic recrystallization of ferrite is possible through a suitable choice of deformation conditions (applied strain, strain rate, and deformation temperature) yielding to ferrite grains finer than 2 μm.

K. MUKHERJEE, formerly Graduate Student with The Centre for Metallurgical Process Engineering, The University of British Columbia, Vancouver, BC, Canada V6T 1Z4, is Postdoctoral Fellow with Institut für Eisenhüttenkunde, RWTH Aachen University, 52072 Aachen, Germany. Contact e-mail: krishnendu.mukherjee@iehk.rwth-aachen.de S.S. HAZRA, formerly Graduate Student with The Centre for Metallurgical Process Engineering, The University of British Columbia, is Ph.D. Student with the Department of Mechanical, Materials and Mechatronics Engineering, University of Wollongong, Wollongong, NSW 2500, Australia. M. MILITZER, Professor, is with The Centre for Metallurgical Process Engineering, The University of British Columbia.
Manuscript submitted May 15, 2008.
Article published online July 14, 2009

To obtain DIFT, strongly undercooled, metastable austenite is heavily deformed in a temperature range that is usually 25 °C to 100 °C above the Ar_3 temperature; *i.e.*, the transformation start temperature for the same cooling path but without the deformation step. As phase transformation is a more favorable reaction as compared to the recrystallization of austenite in this low-temperature regime, deformation at this temperature enhances ferrite nucleation. Significant undercooling below the Ae_3 temperature provides a *sufficiently high driving pressure* for ferrite nucleation. This enhanced ferrite nucleation results in ultrafine ferrite (UFF) grains.[7–26]

Yada *et al.*[9] claimed for the first time that 2-to-3-μm UFF can be formed in a C-Mn steel by deforming in the temperature range from Ar_3 + 50 °C to Ar_3 + 100 °C, when reductions of more than 50 pct have been applied in less than 1 second. There is evidence now that ferrite is formed dynamically from austenite and not during the post-deformation treatment.[10–12] Meanwhile, DIFT has been applied in laboratory tests for a wide variety of steel chemistries, leading rather independent of alloying content to the formation of UFF.[13–15]

Hodgson *et al.* produced 1-μm equiaxed ferrite grains in low-carbon steel by DIFT during the laboratory rolling of thin strip.[16–18] However, the UFF layer is found to be present only in the surface of the strip. According to Hurley *et al.*, microshear bands are produced within the austenite grains during the rolling of austenite and UFF grains are nucleated at cell boundaries within these microshear bands.[19,20] The scale of the dislocation cell structures (~1 μm) is similar to the final UFF grain size.

Beladi *et al.*[21] reported the existence of a critical strain for UFF formation ($\varepsilon_{critical,UFF}$). At strains higher than $\varepsilon_{critical,UFF}$, the final microstructure does not change significantly. Hong *et al.*[22] reported that the critical strain decreases with a decrease in the deformation temperature. The effect of the strain rate on DIFT is less well established. For example, Choi *et al.*[23] indicated that the role of the strain rate is insignificant compared to the role of prior austenite grain size and deformation temperature. However, Hong *et al.*[24] observed that applying a higher strain rate enhances DIFT; Yang *et al.*[25] observed that strain rate influences the amount of deformation required to achieve DIFT. Further, the effect of prior austenite grain size is discussed controversially. Beladi *et al.*[21,26] argue that finer prior austenite grains have more potential for DIFT as compared to larger prior austenite grains, *i.e.*, for finer prior austenite grains, both grain-boundary ferrite and intragranular ferrite coarsened in similar fashion, resulting in a homogeneous final ferrite grain size distribution. In contrast, Hurley *et al.* observed that larger prior austenite grains suppress the formation of grain-boundary proeutectoid ferrite and encourage DIFT.[16]

In general, there is a lack of systematic studies on DIFT and, in particular, such studies have yet to be performed to obtain ultrafine DP steels by DIFT. The goal of the present work is to quantify the grain-refining ability in ferrite-martensite structures by the DIFT technique in selected low-C steels with systematically varied chemistries, starting from a commercial DP 600 chemistry. Different processing conditions are investigated to quantify the effects of the initial austenite grain size, amount of deformation, and deformation temperature on the resulting microstructures.

II. EXPERIMENTAL

A. *Materials and Equipment*

The chemical composition of the steels studied is shown in Table I. In addition, the Ae_3 temperatures reported have been obtained from Thermo-Calc* version N, using the Fe 2000 database.

*Thermo-Calc is a trademark of Thermo-Calc Software, Stockholm, Sweden.

The Mo steel is a DP 600 commercial grade supplied in the form of transfer bar material from an industrial heat. The other grades were laboratory cast and subsequently hot rolled to 23-mm-thick plates. Starting from the DP 600 steel chemistry, the Nb and Mo contents are varied in the other steels, to study the effect of these two alloying elements on DIFT. The Ae_3 temperatures are essentially the same for all four chemistries. This indicates that changing the microalloying content of Mo and/or Nb has, for the investigated range, little effect on equilibrium transformation temperatures.

Laboratory simulations were carried out using a Gleeble 3500 thermomechanical simulator (Dynamic Systems, Inc., Poestenkill, NY) that provides precise control of the strain, strain rate, and heating and cooling rates. The tests were conducted under a vacuum condition of 1.33×10^{-4} Pa (10^{-6} torr). In addition, selected hot torsion tests were performed with a Gleeble HTS 100 machine (Dynamic Systems, Inc.) to simulate hot strip rolling that includes a DIFT pass.

The microstructures obtained in all tests were analyzed by standard metallographic techniques, including optical and scanning electron microscopy (SEM)

Table I. Chemical Composition of Steels Studied (Weight Percent) and Ae_3 Temperature

Steel	C	Mn	Si	Nb	Mo	Ti	Al	N	Ae_3 (°C)
Mo	0.06	1.9	0.08	0.004	0.16	0.01	0.04	0.007	820
Nb	0.06	1.8	0.09	0.06	—	—	0.04	0.006	822
Mo-Nb	0.06	1.8	0.09	0.045	0.15	—	0.06	0.006	823
Plain C	0.057	1.8	0.085	—	—	0.006	0.041	0.0064	821

employing a secondary electron detector. Conventional SEM is sufficient to observe 0.3-μm ferrite grains in the secondary electron mode. However, mapping the microstructure by electron backscattered diffraction (EBSD) using a conventional SEM with a W filament is limited to a resolution of approximately 0.5 μm.[29] Thus, selected microstructures for all four steels were mapped by EBSD using a field-emission gun (FEG)–SEM. The sample preparation for EBSD consists of standard mechanical polishing to 0.05 μm followed by electropolishing in a 5 pct perchloric acid and 95 pct acetic acid solution (by volume) with an applied voltage of 35 V. The HKL Channel 5 system (Oxford Instruments, Abingdon, Oxfordshire, United Kingdom) was used for data acquisition and analysis. A step size of 0.2 μm was employed for the EBSD maps. The ferrite grain sizes were quantified as equivalent area diameter for both conventional SEM and EBSD images. At least 1000 grains were included in each grain size measurement. To obtain an indication of the mechanical properties, hardness measurements were carried out for selected microstructures.

B. *Pretests*

Initial austenite grain sizes were determined for each steel by heating the steel at a rate of 5 °C/s to different austenitizing temperatures, T_γ, and holding there for 2 minutes followed by water quenching. Small rectangular samples with a dimension of 6 × 15 × 3 mm were used for these tests. Prior austenite grain boundaries were revealed by etching with a solution consisting of 2 gm picric acid, 1 mL hydrochloric acid, and 1 gm dodecylbenzenesulfonic acid in 100 mL distilled water at 65 °C for 300 to 600 seconds. Based on these studies, reheating conditions were identified to produce a range of austenite grain sizes that can be expected after finish mill rolling. Subsequently, the austenite-to-ferrite transformation start temperatures during continuous cooling without any deformation were determined using dilatometric measurements, as described elsewhere in detail.[27]

C. *DIFT Test Procedures*

Standard cylindrical samples with a diameter of 10 mm and a length of 15 mm were found to be unsuitable for the DIFT tests that involve rapid cooling steps at rates of 40 °C/s and above. Reducing the cylindrical specimen size was seen to be impractical because of the challenges in conducting controlled tests with these small specimens. Thus, an approach using tensile specimen geometries was adopted that was previously employed for continuous cooling transformation tests involving a deformation step.[30] For the present DIFT tests, a specimen geometry with a cylindrical working zone 10 mm in length and 6 mm in diameter was selected, as illustrated in Figure 1. This rather complex sample geometry was introduced to satisfy the different requirements of these tests, which include deformation and rapid cooling. Rapid cooling is key to establishing a high degree of undercooling. Due to the constrained geometry of the selected sample

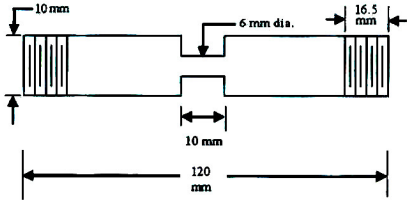

Fig. 1—Specimen geometry for DIFT tests.

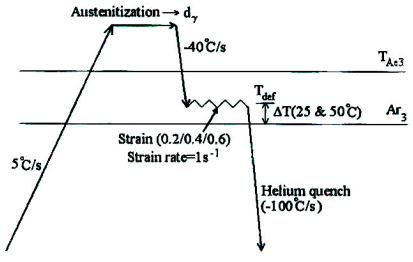

Fig. 2—DIFT test procedure.

design, the strain distribution was not uniform along the axis of the sample. In this study, the reported strain values are the diametrical strains measured in the center plane of the specimen, where the temperature was also recorded.

The thermomechanical path for the DIFT tests is schematically shown in Figure 2. The specimens were first austenitized at the established conditions to form a desired austenite grain size. They were then cooled to the deformation temperature, T_{def}, with a cooling rate of 40 °C/s; this was immediately followed by deformation at a strain rate of 1 s^{-1} to a prescribed diametrical strain. Two sets of deformation temperatures were included in this study, with a temperature difference, ΔT, above Ar_3 that falls into the range of 25 °C to 50 °C. After deformation, the specimens were immediately quenched to room temperature. In general, a He quench with a cooling rate of approximately 100 °C/s was employed. To evaluate the role of the quench rate, a water quench was applied in selected cases. The water quench resulted in an average surface cooling rate of approximately 400 °C/s, while the cooling rate in the center of the specimen was estimated to be approximately 300 °C/s, considering heat conduction in an infinitely long cylinder, in which heat flow occurs only in the radial direction. These post-deformation cooling rates are larger than the critical cooling rates observed by Liu *et al.*[28] to form martensite as secondary phase when the polygonal ferrite fraction is 0.7 and higher. The data of Liu *et al.* indicate that, for the Mo steel, for example, these critical cooling rates are below 10 °C/s

but can be as high as 100 °C/s in plain-carbon steel (0.07 wt pct C, 1.45 wt pct Mn, and 0.73 wt pct Si).

Hot torsion tests were carried out using standard procedures, as described elsewhere in more detail.[28] The present torsion tests were modified by including a DIFT pass during the cooling step after the simulation of a seven-stand finish mill.

III. RESULTS

A. *Austenite Grain Size and Transformation Start Temperatures*

The results of the pretests are summarized in Table II. In all steels, increasing the reheat temperature results in a larger austenite grain size, d_γ. In the microalloyed steels, a gradual grain size increase is observed from 10 to 15 μm for reheating at 950 °C to approximately 25 μm for reheating at 1100 °C. However, for the plain-carbon steel, a more abrupt grain-coarsening behavior occurs. At the lower reheat temperature of 950 °C, revealing the austenite microstructure proved to be challenging in this steel such that only a grain size estimate (≤20 μm) can be provided. Further, for this steel, a reheating condition that gives a homogeneous grain size of approximately 30 μm could not be established. Increasing the reheating temperature from 950 °C results in rapid coarsening of the austenite microstructure by abnormal grain growth, presumably due to the dissolution of AlN.[31] Thus, the 1200 °C reheat condition that results in a homogeneous microstructure with an austenite grain size of approximately 70 μm has been included in the present study.

Table II. Summary of Pretest Result

Steel	T_γ (°C)	d_γ (μm)	Ar_3 (°C)	Ae_3-Ar_3 (°C)
Mo	950	13	670	150
	1050	20	655	165
	1100	27	650	170
Nb	950	11	647	175
	1100	25	504	318
Mo-Nb	950	10	602	221
	1100	26	528	295
Plain C	950	20*	650	171
	1200	68	575	246

*Estimate.

For all steels, the Ar_3 temperature decreases with increasing initial austenite grain size. Strong effects of Nb can be seen in delaying ferrite formation. This effect is more pronounced for larger austenite grain sizes, which are obtained by increasing the reheat temperature from 950 °C to 1100 °C, thereby also increasing the amount of Nb in solution.

Typically, an undercooling of 150 °C to 180 °C is observed for the Ar_3 temperatures after reheating at 950 °C, except for the Mo-Nb steel, in which this undercooling is in excess of 200 °C. For higher reheat temperatures, the level of undercooling is increased to 250 °C or above in the Nb-containing steels and also in the plain-carbon steel, for which reheating at 1200 °C results in a significantly larger austenite grain size (*i.e.*, 70 μm).

B. *Effect of Alloying Elements and Processing Conditions on DIFT Microstructures*

In the DIFT tests, increasing the amount of applied strain increases the amount of UFF, for all chemistries. For a true strain, ε, of 0.6 applied to the finer prior austenite grain size, the microstructure contains 70 pct or more ultrafine-grained ferrite, indicating that this strain level is the critical strain required to obtain a predominantly ultrafine ferritic structure. Although UFF can be obtained in all four steels, the evolution of microstructure with applied strain varies for different chemistries.

In the plain-carbon steel, employing the lowest amount of applied strain resulted in a microstructure with a ferrite fraction of 0.65 consisting of both large and fine ferrite grains. Applying a larger amount of strain increased the fine-grained ferrite fraction (Figures 3(a) and (b)). In contrast, applying the lowest amount of

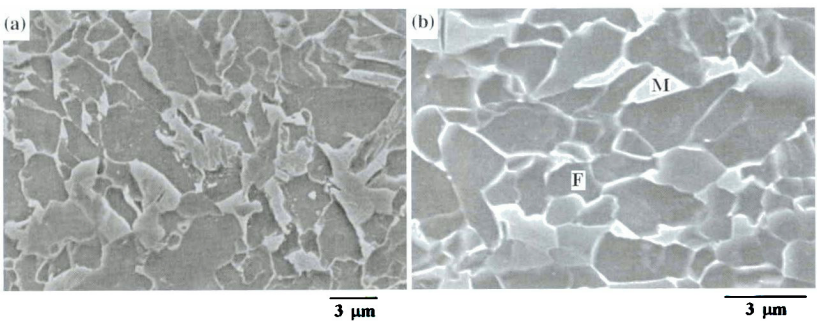

Fig. 3—Effect of strain on microstructure for plain-C steel reheated at 950 °C and deformed at ΔT = 25 °C: strain = (*a*) 0.23 and (*b*) 0.67.

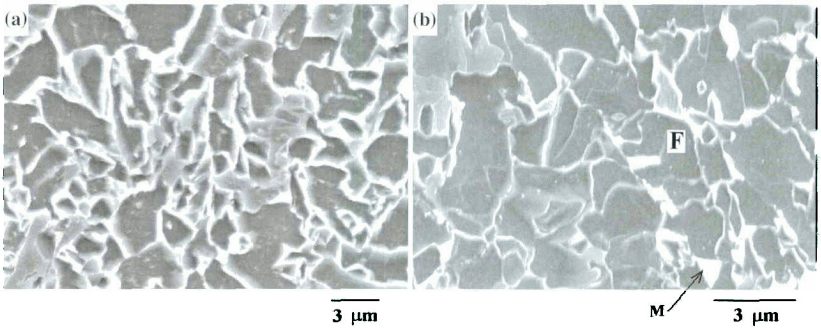

Fig. 4—Effect of strain on microstructure for Nb steel reheated at 950 °C and deformed at ΔT = 25 °C: strain = (*a*) 0.2 and (*b*) 0.6.

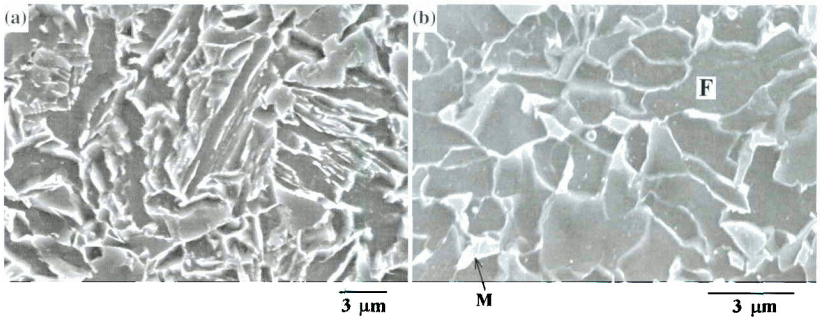

Fig. 5—Effect of strain on microstructure for Mo-Nb steel reheated at 950 °C and deformed at ΔT = 25 °C: strain = (*a*) 0.2 and (*b*) 0.6.

strain for the Nb steel resulted in an insignificant fraction of ferrite. Increasing the amount of strain led to the progressive formation of ferrite, with a simultaneous decrease in grain size (Figures 4(a) and (b)). Similarly, for the Mo-Nb steel, the microstructure contained an insignificant amount of ferrite, even for a strain of 0.4. However, with the highest amount of strain (*i.e.*, 0.6), an ultrafine ferritic structure was obtained (Figures 5(a) and (b)). Figure 6 summarizes the effect of strain on the resulting microstructure for the Mo steel with a prior austenite grain size of 20 μm and a deformation temperature of 685 °C. A strain of 0.15 introduces some ferrite grains, as shown in Figure 6(a). Raising the applied strain to 0.35 increases the ferrite fraction (Figure 6(b)). A strain of 0.55 is sufficient to produce a predominantly fine-grained ferrite microstructure. However, a few comparatively large ferrite grains can be observed, as well (Figure 6(c)). In Figures 3(b), 4(b), 5(b), and 6(c), labels are added to better identify different phases. In those figures, F indicates ferrite and M indicates martensite.

The effect of deformation temperature on DIFT was studied for the highest amount of deformation with a true strain of approximately 0.6 applied to the smallest prior austenite grain size (~10 to 15 μm). Figure 7 summarizes the effects of the deformation temperature on DIFT in terms of the ferrite fraction and grain size of the final microstructures. The major effect of increasing the deformation temperature from 25 °C to 50 °C above Ar_3 is that, except for the Mo steel, the ferrite fraction decreases by approximately 10 pct (Figure 7). However, there is a marginal effect of deformation temperature on the final average ferrite grain size, d_α, that in all cases falls into the range of 1 to 1.5 μm.

The Nb-containing steels show a lower tendency to form UFF, due to the delaying effect of Nb on ferrite transformation. This is more pronounced for larger initial austenite grain sizes that result from reheating at 1100 °C, at which temperature it is expected that some of the Nb-containing precipitates will dissolve. For Nb and Mo-Nb steels, increasing the initial austenite grain size to approximately 25 μm results in marginal ferrite

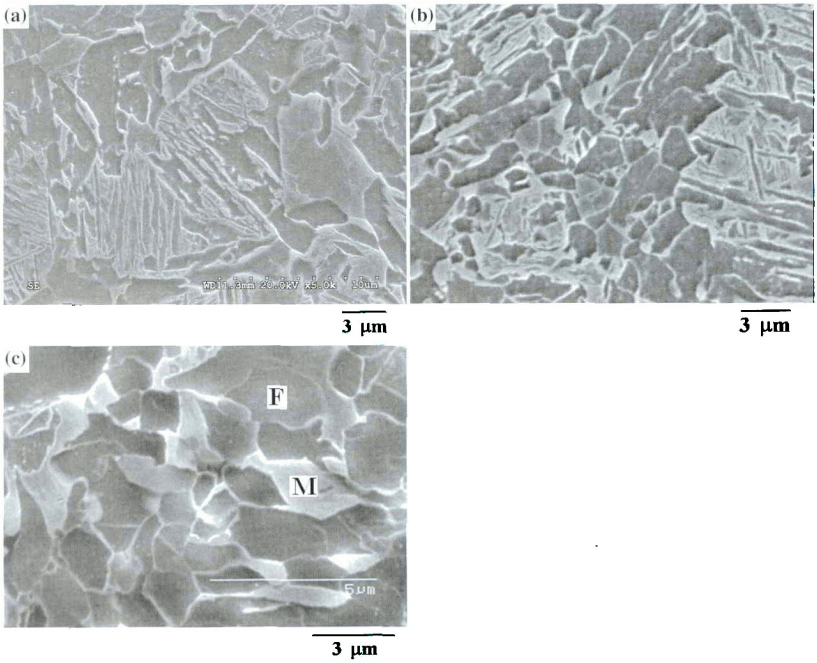

Fig. 6—Effect of strain on microstructure for Mo steel reheated at 1050 °C and deformed at ΔT = 30 °C: strain = (*a*) 0.15, (*b*) 0.35, and (*c*) 0.55.

fractions below 0.2, even with the highest employed strain of 0.6. The Ar_3 temperatures for the larger prior austenite grain size of Nb and Mo-Nb steels are below 550 °C and, thus, they are below the polygonal ferrite formation region, *i.e.*, Ar_3 temperatures indicate transformation start for nonferritic transformation products in these cases. For the Mo steel, increasing the initial austenite grain size has minor effects on the final microstructure. For example, when ΔT = 50 °C and ε = 0.6, the UFF decreases from 85 to 81 pct when the austenite grain size increases from 13 to 27 μm. This is due to the fact that this increase in austenite grain size reduces the Ar_3 temperature by 20 °C only, as seen in Table II. Nevertheless, in general, a finer prior austenite grain size appears to promote the formation of UFF.

C. *Predominantly UFF Microstructure*

In the present study a significant amount of UFF, *i.e.*, 70 pct or more in the final microstructure, is obtained in all investigated steels when the highest amount of deformation with a true strain of approximately 0.6 is applied to the finest initial austenite grain size in the range of 10 to 15 μm. The results of these tests are summarized in Figure 7. As indicated earlier, a predominantly UFF microstructure is also obtained in the Mo chemistry steel for a larger initial austenite grain size of 27 μm. In all cases, the ferrite grain size is ~1 μm and a lognormal ferrite grain size distribution is observed. As an example, the ferrite grain size distribution for the Mo steel austenitized at 950 °C (d_γ = 13 μm) and subsequently deformed at 695 °C (Ar_3 + 25 °C) is plotted in Figure 8. The bar chart in the figure shows the measured grain size distribution, while the solid line represents the log-normal fit of the distribution at which the frequency $f(x)$ of grains with a diameter x is given by

$$f(x) = \frac{1}{x\sigma\sqrt{2\pi}} \exp\left(\frac{-\{\ln(x/x_m)\}^2}{2\sigma^2}\right) \quad [1]$$

Here, σ is the standard deviation and x_m is the median grain size. As summarized in Table III, the distributions are very similar in all steels, with x_m being approximately 1 μm and σ values being 0.6 ± 0.1.

In the context of the present work, the optimized microstructures with a maximized amount of UFF are obtained for all four steels when the smallest prior austenite grain size is selected and the highest amount of

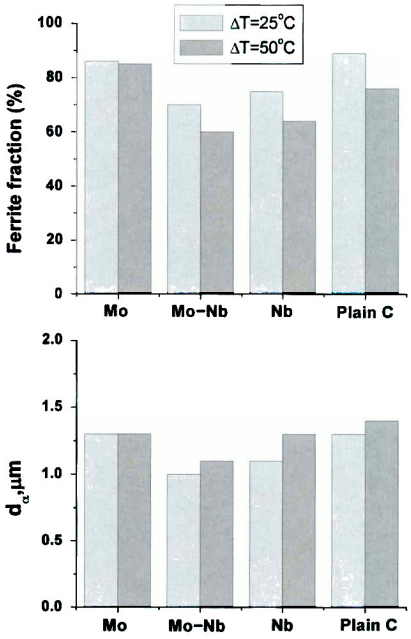

Fig. 7—Ferrite fraction and grain size for each steel when reheated to 950 °C and deformed to a true strain of 0.6 ± 0.05.

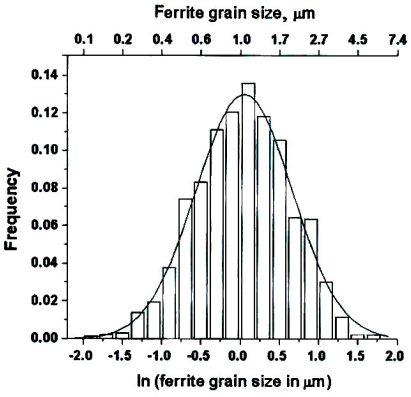

Fig. 8—Grain size distribution for Mo steel as measured (d_i = 13 μm, T_{def} = 695 °C, ε = 0.65) and as-fitted log-normal distribution (solid line).

Table III. Data Representing Log-Normal Distribution for UFF

Steel	T_γ (°C)	Deformation Temperature (°C)	x_m	σ
Mo	950	695	1.0	0.61
		720	1.0	0.60
	1050	685	1.1	0.56
	1100	700	0.9	0.65
Nb	950	672	1.0	0.56
		697	1.1	0.65
Mo-Nb	950	627	0.9	0.50
		652	1.0	0.59
Plain C	950	675	1.1	0.59
		700	1.2	0.65

strain is applied at ΔT = 25 °C. These microstructures have been selected for further analysis by EBSD mapping. Figure 9 shows the orientation maps of all four steels. The colors indicate the crystal direction parallel to the compression direction of the samples. High-angle boundaries with a misorientation of 10 deg or more, and low-angle boundaries with a misorientation of 2 to 10 deg are indicated by thick and thin black lines, respectively. The lower limit of measurable grain-boundary misorientation angles has been taken as 2 deg. The scheme for obtaining the EBSD maps shown in Figure 9 from the as-measured raw data is described in the Appendix, in which details are also provided for the procedures for identifying different phases and obtaining the ferrite grain size from the EBSD data.

The ferrite grain sizes obtained from EBSD studies are compared in Table IV with those obtained from the conventional SEM studies. It can be seen that the ferrite grain sizes determined by the EBSD analysis, using a critical misorientation angle of 2 deg to define grains, are similar to those determined by conventional SEM studies. The discrepancy between the ferrite grain sizes obtained by the EBSD analysis with a critical misorientation angle of 2 deg and those obtained by SEM studies is greatest in the case of Nb steel. It is interesting that, for the Nb steel, the EBSD grain sizes are virtually independent whether a misorientation angle of 2 or 10 deg is employed to identify grains, whereas for the other steels, a substantial increase in the apparent grain size, from 1.3 through 1.5 μm to 1.9 through 2.1 μm is recorded when the critical misorientation is raised to 10 deg, which is characteristic of high-angle grain boundaries.

To further appreciate these details, it is worthwhile considering the distributions of the grain-boundary misorientation angles that are shown in Figure 10 for the four EBSD maps. These distributions confirm that the Nb steel has a higher proportion of high-angle grain boundaries (grain boundaries with a misorientation angle of 10 deg or more) as compared to the other steels. In detail, it can be seen from Figure 10 that, in the Nb steel, just 15 pct of the grain boundaries are low-angle boundaries with misorientations below 10 deg, whereas in all other steels, 40 to 45 pct of the grain boundaries have misorientation angles between 2 and 10 deg. This is consistent with the observation of clusters

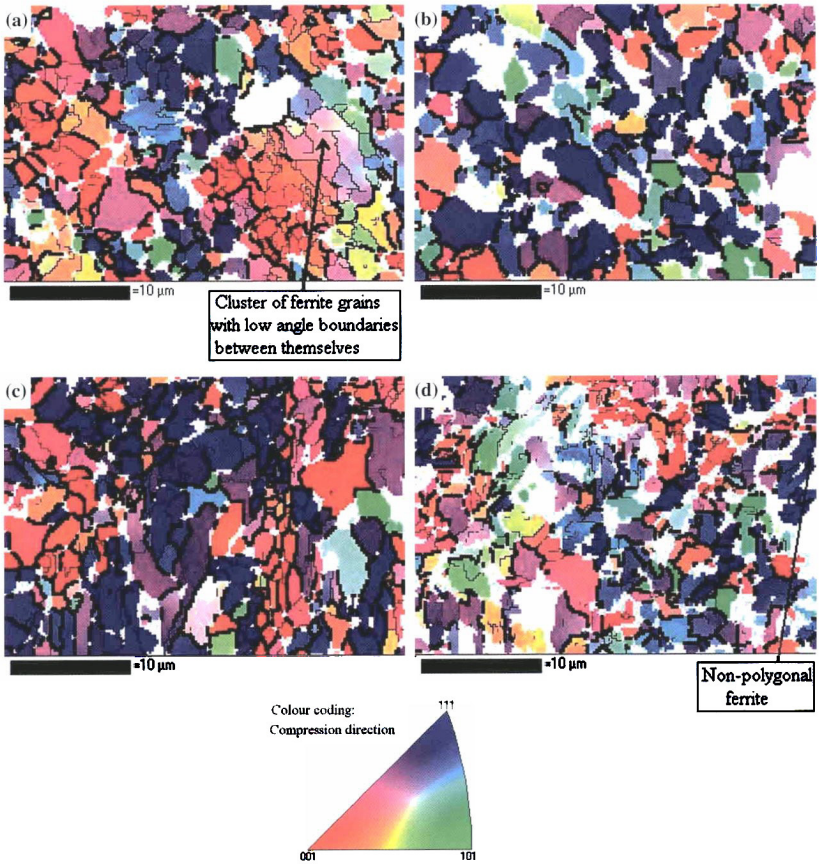

Fig. 9—EBSD maps for optimized conditions for all steels (thick black lines indicate boundaries with misorientation ≥10 deg, thin black lines indicate boundaries with misorientation of 2 to 10 deg, and white areas indicate second phases as described in the Appendix): (*a*) Mo steel, (*b*) Nb steel, (*c*) plain-C steel, and (*d*) Mo-Nb steel.

Table IV. Mean Ferrite Grain Sizes Obtained from EBSD and Conventional SEM for Optimized Cases

Steel	d_z (μm) EBSD (Critical Misorientation Angle = 2 Deg)	d_z (μm) EBSD (Critical Misorientation Angle = 10 Deg)	d_z (μm) Conventional SEM
Mo	1.3	1.9	1.3
Plain C	1.5	2.1	1.3
Nb	1.8	1.9	1.3
Mo-Nb	1.3	1.9	1.0

of ferrite grains with low-angle boundaries between themselves for the Mo, plain-C, and Mo-Nb steels. A typical example of this kind of cluster of ferrite grains is shown in Figure 9(a). However, such grain clusters are not observed in the Nb steel.

D. *Effect of Post-Deformation Cooling Rate*

The Mo steel is further selected to study the effect of the post-deformation cooling rate. The post-deformation cooling rate is increased to enhance the martensite

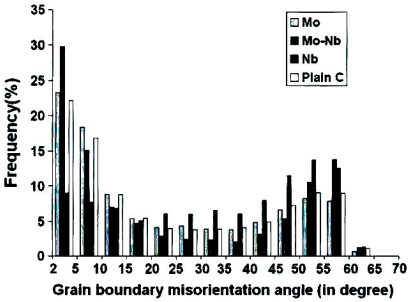

Fig. 10—Distribution of grain-boundary misorientation angle for optimized conditions in all four steels.

formation after DIFT. The delay time in starting the quench after deformation is 0.1 and 0.4 seconds for the He quench and water quench, respectively. The amount of martensite is increased from 14 pct for He quenching (post-deformation cooling rate of 100 °C/s) to 28 pct for water quenching (post-deformation cooling rate of 300 °C/s), with an insignificant change in ferrite grain size. This indicates that some ferrite forms during cooling (or post-deformation holding). For the Mo steel, a post-deformation cooling rate of 100 °C/s appears to be adequate for forming a desirable UFF-martensite microstructure with a martensite fraction of approximately 15 pct. However, further studies are required to establish in more detail the post-deformation cooling conditions for the desired ferrite-martensite DP structures.

E. *Mechanical Properties*

The DIFT specimen geometry is not suitable for performing standard tensile tests. Thus, hardness measurements are taken to obtain an indication of the mechanical properties for selected UFF microstructures. Table V summarizes the hardness data and the predicted flow stress at 8 pct strain ($\sigma_{0.08}$) estimated from Tabor's relation:[32]

$$H_V = 3\sigma_{0.08} \qquad [2]$$

where H_V is the Vicker's hardness. The Vicker's hardness number is in kg/mm^2 such that a unit conversion factor has to be introduced into Eq. [2] to obtain the flow stress in MPa (1 H_V = 9.81 MPa).

Table V. Summary of Hardness Measurements for Optimized Conditions

Steel	H_V	Predicted $\sigma_{0.08}$ (MPa)
Mo	204 ± 3	667 ± 10
Nb	248 ± 3	811 ± 10
Mo-Nb	278 ± 6	909 ± 20
Plain C	206 ± 3	674 ± 10

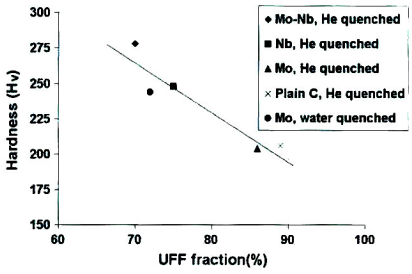

Fig. 11—Hardness as a function of UFF fraction for fine-grained DP microstructures.

The predicted stress levels support the potential of refining microstructures to obtain DP steels with tensile strength levels much in excess of the 600 MPa of the currently most widely utilized DP steels. As shown in Figure 11, hardness values decrease linearly as the UFF fraction increases. The two data points for the Mo steel follow the trend for all other steels, indicating that the higher strength levels in the Nb-containing steels are primarily related to their higher fraction of secondary transformation products rather than to potential strengthening due to NbC precipitates; the employed processing paths offer few if any opportunities for fine carbides to form.

F. *Torsion Simulations*

The plain-carbon chemistry has been selected to evaluate suitable procedures for the hot strip rolling of ultrafine DP steels with hot torsion simulations. First, the conditions of the Gleeble 3500 tests were replicated with torsion tests using the same time-temperature path with reheating at 950 °C and a deformation temperature of 675 °C. Because deformation in torsion is less efficient in forming UFF by DIFT compared to plain-strain compression (rolling) and axisymmetric compression, a significantly higher amount of deformation has to be applied to produce an UFF microstructure by DIFT in hot torsion.[17] Increasing the amount of equivalent strain from 0.6 to 1.5 increases the fraction of finer ferrite grains, which is similar to the effect of strain on the ferrite grain size observed in the Gleeble 3500 tests. An equivalent strain of 1.5 produces a suitable UFF microstructure, and increasing the equivalent strain to 3.0 does not further refine the microstructure. In both cases, the UFF fraction is approximately 0.9 and the ferrite grain size is 1.7 μm, which is slightly larger than that of the 1.3 μm observed for axisymmetric compression.

A simulation schedule previously proposed for hot-rolled DP steels[28] that consists of reheating for 15 minutes at 1200 °C followed by one roughing and seven finishing passes executed in the austenite region was then modified for the DIFT treatment by adding an

eighth finishing pass (Table VI). After F7, the sample was cooled at 40 °C/s to a selected DIFT pass temperature (*i.e.*, 675 °C and 650 °C, respectively) at which it was deformed to an equivalent strain of 1.5 and subsequently cooled at approximately 30 °C/s. The stress-strain curves of the DIFT passes are shown in Figure 12. Here, the flow stress increases initially rapidly and shows at higher strains dynamic softening that can readily be attributed to ferrite formation during deformation. This flow stress behavior provides some evidence that a significant volume fraction of ferrite forms during deformation as opposed to immediately after deformation. The final microstructures are shown in Figure 13 confirming that this treatment resulted in a UFF microstructure with a ferrite fraction of 0.84 and a grain size of 2 μm for the DIFT pass at 675 °C, while for the DIFT pass at 650 °C, an even finer ferrite grain size of 1.3 μm is observed, with a ferrite fraction of 0.90. For the torsion samples, the cooling rate is limited (~30 °C/s) after the final DIFT pass. As a result, secondary transformation products are expected to contain little martensite.

Table VI. Simulated Rolling Schedule for DIFT

Deformation Pass	Temperature (°C)	Reduction (Pct)	Equivalent True Strain	Interpass Time (s)
R	1150	60	1.05	10
F1	1100	45	0.69	4.8
F2	1060	38	0.55	3.1
F3	1020	33	0.46	2.2
F4	980	30	0.41	1.6
F5	950	27	0.36	1.2
F6	920	23	0.30	0.9
F7	895	20	0.26	5.5/6.1
DIFT	675/650	73	1.50	—

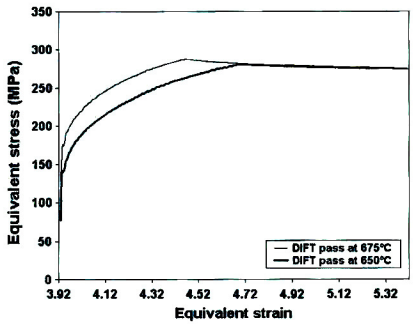

Fig. 12—Stress-strain curve of DIFT passes during hot strip rolling simulation of plain-C steel.

IV. DISCUSSION

A. *Effect of Strain on DIFT*

Increasing the amount of strain increases the potential for DIFT. The increase in strain affected the final microstructure in one of the following ways: (1) a predominantly coarse-grained ferrite microstructure changes to a predominantly fine-grained ferrite microstructure or (2) the fraction of ferrite increases.

In this study, it is observed that for the plain-C steel, increasing the strain gradually replaces coarse-grained ferrite with fine-grained ferrite and, simultaneously, the overall ferrite fraction increases. This is similar to the findings of Hong *et al.*[33] for DIFT in plain-C steel with a fine prior austenite grain size. In Figure 14, the volumetric grain size distribution of ferrite grains are plotted for different amounts of strain. Using the frequency distribution $f(x)$, the volume fraction of grains with size x is given by

$$f_V = \frac{x^3 f(x)}{\int_0^\infty x^3 f(x)dx} \quad [3]$$

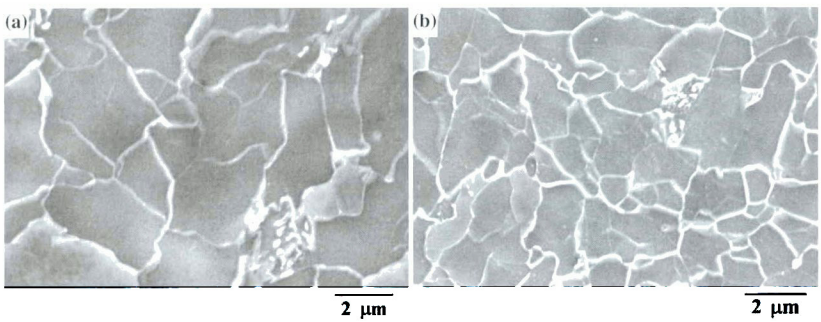

Fig. 13—Simulated hot strip rolling microstructure of plain-C steel with final DIFT pass at (*a*) 675 °C and (*b*) 650 °C.

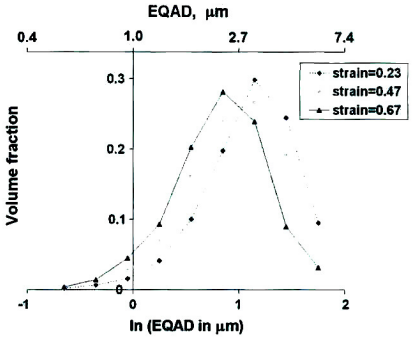

Fig. 14—Volumetric ferrite grain size distributions for plain-C steel obtained in Gleeble DIFT tests with different strains.

From Figure 14, it is observed that the fraction of fine-grained ferrite increases and that of coarse-grained ferrite decreases as the applied strain is increased.

For the other three steels, the fraction of ferrite increases with applied strain and the predominantly nonpolygonal microstructure for lower strain levels is gradually transformed to an ultrafine-grained ferrite structure, by increasing the amount of applied strain. However, the ferrite grain size varies within the length scale of a typical prior austenite grain, *i.e.*, some comparatively large ferrite grains (3 to 4 μm) can be observed within the otherwise ultrafine-grained ferrite (Figure 6(c)). This suggests a variable ferrite nuclei density within a given austenite grain. Consistent with the observations by Beladi *et al.*[26] this may be attributable to a larger nuclei density near the prior austenite grain boundaries and a lower nuclei density within the prior austenite grain.

B. *Effect of Prior Austenite Grain Size on DIFT*

Finer prior austenite grains promoted the formation of an UFF microstructure. However, depending on the steel chemistry, coarser austenite grain structures affected the final microstructures differently. For the Nb-containing steels, increasing the prior austenite grain size retards the DIFT potential. This is in accordance with the findings of Hong *et al.*[24] In contrast, Hurley *et al.* reported increased DIFT potential for increased prior austenite grain size.[16] In the Mo steel, the initial austenite grain size has a marginal effect on the final microstructure. Even though prior austenite grain sizes have not been quantified in detail for the plain-carbon steel, the production of UFF in torsion simulations with different processing in the austenite region suggests that, for this steel also, a range of prior austenite grain sizes can be used to obtain suitable DIFT microstructures.

In analyzing the role of the prior austenite grain size, it has to be considered that changing the austenite grain size also changes the Ar_3 temperature, which in turn affects the deformation temperature in the DIFT schedule. In particular, for the Nb-containing steels, bainite rather than ferrite forms at Ar_3 when d_γ is increased. The higher reheating temperature employed to obtain larger d_γ is expected to bring a significant amount of Nb into solution. The combined effects of larger d_γ and more Nb in solution result in a pronounced delay in the ferrite formation. Hence, austenite grain size cannot be considered as an independent parameter in the DIFT process.

C. *Effect of Steel Chemistry on DIFT*

For plain-C steel, dynamic ferrite nucleation and growth occurs at all levels of applied strain. The nucleation density is lower, in the case of lower strain leading to larger ferrite grains. This behavior is indicative of a relatively fast migration rate of the austenite-ferrite interface. The lowest amount of strain of 0.2 resulted in an insignificant ferrite fraction for the Nb steel. A comparison with the results of the plain-carbon steel, for which essentially the same DIFT temperatures were employed (*i.e.*, 672 °C *vs* 675 °C) may suggest that, in the Nb steel, the velocity of the austenite-ferrite interface is much lower. This hypothesis is consistent with the well-established observation that Nb slows down ferrite transformation rates. In the cases of higher reheating temperatures, a significant amount of Nb goes into solution (a reheating temperature of 950 °C *vs* a reheating temperature of 1100 °C). This results in a pronounced delay in ferrite formation.

The retarding effect of Nb on the transformation rates is also confirmed when comparing the Mo-Nb steel with the Mo steel. For a given strain level, less ferrite is formed in the Mo-Nb steel, consistent with Nb microalloying. Further, the partly nonpolygonal nature of the ferrite grains (example shown in Figure 9(d)) in this steel results from the comparatively low deformation temperature (627 °C), *i.e.*, the undercooling below the Ae_3 temperature is 220 °C here compared to 150 °C to 170 °C for all other steels.

The EBSD studies show that, in Mo, Mo-Nb, and plain-C steels, clusters of ferrite grains form with low-angle boundaries between themselves (example shown in Figure 9(a)). Consequently, an appreciable fraction of low-angle boundaries are present in these DIFT microstructures, as quantified in the distribution of grain-boundary misorientation angles (Figure 10). However, for the Nb steel, the fraction of low-angle boundaries is noticeably lower than in the other steels. More investigations will be required to provide further insight into the relevance of the frequency of low-angle boundaries.

D. *Ferrite Grain Refinement by DIFT*

The Mo steel has a typical DP600 chemistry that had been developed for cold-rolled and annealed DP steels.[34] An extensive database is available for the microstructure evolution in this steel that is applicable

to the currently employed commercial processing routes, *i.e.*, hot rolling and intercritical annealing, to produce DP steels.[28,35,36] Thus, this steel is selected to evaluate the grain-refinement potential of DIFT, as compared to conventional techniques. A typical microstructure obtained by the intercritical annealing route consists of 82 pct ferrite with a grain size of 6 μm.[35] On the other hand, a typical microstructure obtained by hot rolling simulation of the Mo steel (prior austenite grain size of 13 μm) consists of 81 pct ferrite with a grain size of 8.6 μm.[28] In the case of thermomechanically controlled processing, the prior austenite grain size, amount of deformation, and subsequent cooling rate determine the final microstructure. An optimum combination of the finest prior austenite grain size of 13 μm, an applied strain of 0.5 at 850 °C, and a subsequent cooling rate of 60 °C/s resulted in a ferrite grain size of 3.5 μm with a ferrite fraction of 84 pct, which is the finest ferritic microstructure obtained in the set of simulations reported in the literature.[36] Clearly, DIFT can produce a predominantly ferrite microstructure with a considerably finer final ferrite grain size, as compared to conventional techniques.

E. *Predicted Improvement in Mechanical Properties*

To evaluate the strength increase by grain refinement, hardness data can be used. In Table VII, the hardness values for the Mo steel that has several coarse-grained DP microstructures are compared with the hardness value for the fine-grained DP microstructure produced by DIFT. These data confirm the clear trend that refining the microstructure increases the strength levels. For example, a hardness value of 167 HV is obtained for the conventional DP microstructure obtained by simulation of cold rolling and annealing. In contrast, in the DIFT sample, a hardness of 204 HV has been recorded. This indicates a tensile strength increase of 20 pct from the observed grain refinement of 6 to 1 μm.

F. *Industrial Applicability of DIFT to Produce Fine-Grained DP Steel*

The simulation of industrial DIFT processing with hot torsion tests for the plain-C steel gives promising results for realizing UFF microstructures in as-hot-rolled plain-carbon steels, *i.e.*, without the addition of costly alloying elements. The applied strain in the DIFT pass may appear excessive, but this is just an artifact of the torsion deformation mode that appears to be less efficient in introducing viable ferrite nucleation sites at microshear bands. For rolling, a reduction of approximately 35 pct (true strain 0.5) can be expected to be sufficient for this purpose. Even so, the proposed schedule is beyond the capabilities of conventional hot strip mills. An additional mill stand would have to be added in the runout table area. This could be considered in new mill designs, but will first require a detailed assessment of the robustness of the proposed processing path. Alternatively, recent work by Morimoto *et al.*[37] suggests that DIFT can be initiated in the final stands of a seven-stand finish mill by proper interstand cooling in conjunction with asymmetric rolling that produces significant shear strain to reach the critical strain levels for UFF formation. In any event, a distinct advantage of the DIFT route would be that ferrite forms very rapidly within less than 1 second, thereby eliminating the need for a slow cooling period of more than 10 seconds through the ferrite formation stage that is usually employed in the current production of hot-rolled DP steels.

Table VII. Comparison of Hardness in Mo Steel with Fine- and Coarse-Grained DP Microstructures

d_α (μm)	Ferrite Fraction	Hardness (H_V)
10	0.84	145
6	0.82	167
3.5	0.84	172
1.3	0.86	204

V. CONCLUSIONS

The DIFT can be successfully used to form UFF for all investigated chemistries, provided suitable processing conditions are applied. The DIFT produces finer ferrite grain sizes as compared to conventional DP microstructures with similar martensite fractions. Increasing the amount of applied strain increases the potential for DIFT. For all four chemistries, increasing the deformation temperature from 25 °C to 50 °C above Ar_3 results in an insignificant effect on the final ferrite grain size. The major effect of increasing the deformation temperature is a decrease in the ferrite fraction by approximately 10 pct. In the cases of the Nb and Mo-Nb microalloyed steels, a fine prior austenite grain size (~10 μm) is required to produce a predominantly UFF microstructure. But for the Mo steel, a predominantly UFF microstructure is also obtained from larger prior austenitic grain structures (d_γ = 27 μm). Even though prior austenite grain sizes have not been quantified in detail for the plain-carbon steel, the production of UFF in Gleeble and torsion simulations with different processing in the austenite region suggests that, for this steel also, a range of prior austenite grain sizes can be used to obtain suitable DIFT microstructures. However, rapid cooling, *e.g.*, 100 °C/s, after the DIFT deformation step is key to the plain-carbon steel obtaining martensite as a secondary transformation product, thereby attaining the desired fine-grained DP microstructure.

Among the four chemistries studied, the plain-C and Mo steels appear to be potential candidates for industrial production, because moderate changes in the deformation temperature and austenite grain size result in similar UFF fractions. This would be well suited to design a reasonably stable industrial processing window. Further evaluation is needed for the plain-C steel with systematic variation of the initial austenite microstructure. Adding Nb tends to retard the formation of UFF by DIFT, but this may be mitigated when applying DIFT on work-hardened austenite.

ACKNOWLEDGMENTS

The financial support received from project C05-CST of Canada's National Centre of Excellence (NCE) AUTO21 and the Natural Sciences and Engineering Research Council of Canada is acknowledged with gratitude. The Mo steel was supplied by Stelco Inc. (now U.S. Steel Canada Inc., Hamilton, ON, Canada) and the laboratory steels by CANMET Materials Technology Laboratory of Natural Resources Canada (Ottawa, ON, Canada). The authors thank Peter Hodgson and Andrew Sullivan for carrying out the EBSD mappings, Chad Sinclair for inspiring discussions, and Hamid Azizi-Alizamini for assistance in the metallographic work.

APPENDIX

Analysis of EBSD maps

The analysis of the EBSD maps is described using the example of the Mo steel shown in Figure 9(a). Figure A1 shows the original EBSD map. In all figures of the Appendix, unless mentioned otherwise, the colors indicate the crystal direction parallel to the compression direction of the samples (color coding is shown in Figure 9). The unindexed white pixels indicate either a nonferritic phase or a grain-boundary region. In analyzing these as-obtained maps, unindexed points are extrapolated to indexed points using a standard Channel 5 technique (Figure A2). This clean-up step involves in sequence an 8-neighbor extrapolation, a 7-neighbor extrapolation, and again another 8-neighbor extrapolation. Then objects are determined based on a selected critical misorientation, *e.g.*, 2 deg (Figure A3). In Figure A3, the objects are shown in random colors.

One of the challenges is that ferrite and martensite have a similar crystal structure that cannot be crystallographically distinguished based on EBSD. However, band contrast can be used to separate the two phases. Band contrast indicates the sharpness of the Kikuchi pattern obtained from the diffraction of the incident electron beam. A deviation from the perfect crystalline structure will result in a diffused Kikuchi pattern with a low band contrast value. Because martensite is inherently a more defect-containing structure as compared to ferrite, it is expected to have a lower band contrast. Hutchinson *et al.*[38] and Waterschoot *et al.*[39] utilized a similar parameter, image quality, to distinguish ferrite from other transformation products. Zäfferer *et al.*,[40] however, argued that using high-resolution FEG-SEM results in similar pattern quality for ferrite and bainite. The band-contrast distribution for the present EBSD map is shown in Figure A4. Clearly, a shoulder in the distribution is visible, indicating that two different object types contribute to this distribution.

To classify objects, the mean band contrast of each object is determined (Figure A5). A critical mean band contrast ($BC_{critical}$) is determined such that objects having a mean band contrast above $BC_{critical}$ are considered to be ferrite and the rest can be considered as martensite. No general, independent value of $BC_{critical}$ can be established, as band contrast also depends on sample preparation. Thus, the martensite fraction

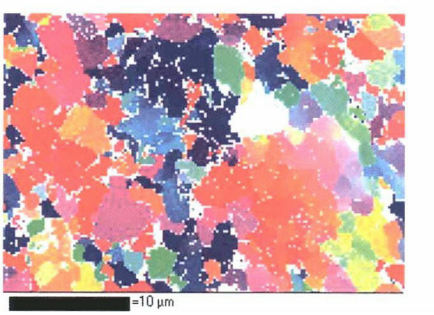

Fig. A1—Original EBSD map for Mo steel.

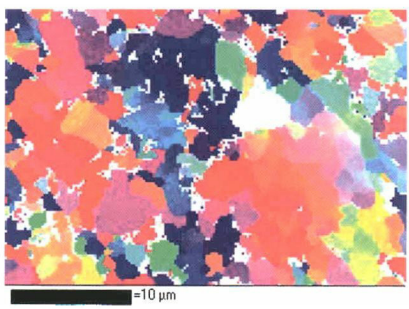

Fig. A2—Map obtained after cleaning of map shown in Fig. A1.

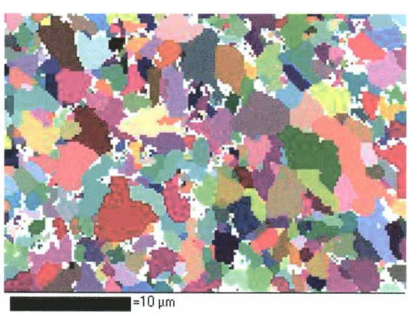

Fig. A3—Object determined based on critical misorientation of 2 deg for map shown in Fig. A2.

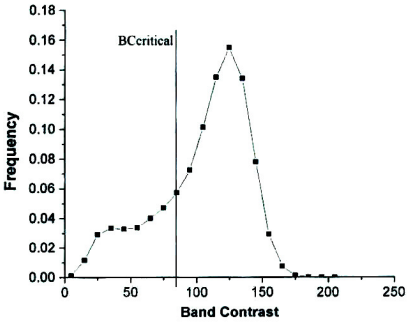

Fig. A4—Band contrast distribution with $BC_{critical}$ for the EBSD map of Mo steel.

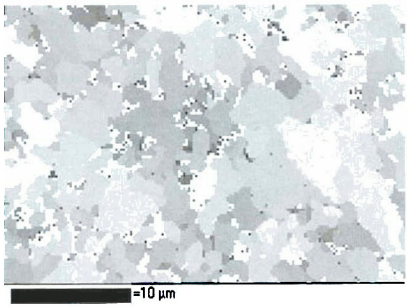

Fig. A5—Mean band contrast map for the Mo steel.

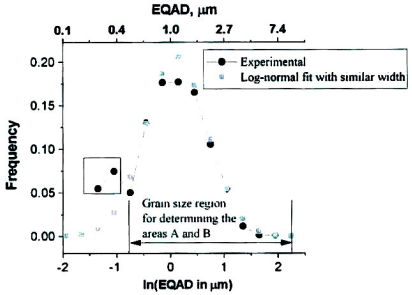

Fig. A6—Grain size distribution obtained from the EBSD map for Mo steel (critical misorientation angle is 2 deg and $BC_{critical}$ is 85) and as-fitted log-normal distribution with similar width and ignoring the noise.

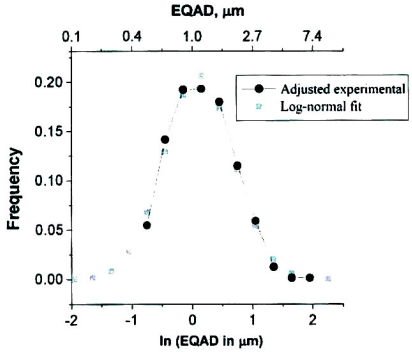

Fig. A7—Adjusted grain size distribution and refitted log-normal distribution by ignoring the noise.

determined from conventional SEM has been used to quantify $BC_{critical}$ such that the martensite fraction obtained in conventional SEM studies is equal to the sum of the fraction of nonindexed points and the fraction of objects below $BC_{critical}$.

The value of $BC_{critical}$ determined for the present EBSD map is indicated in Figure A4 and corresponds reasonably well with the position of the shoulder in the distribution. The objects having a mean band contrast greater than 85, which is the value of $BC_{critical}$, for the present EBSD map, are considered as ferrite grains. Figure 9(a) is the final processed EBSD map, in which the colored objects represent ferrite grains and white regions indicate the second phase.

The ferrite grain size distribution graph obtained from the processed EBSD map is shown in Figure A6. The region indicated by the rectangular box in the figure is due to the noise (*i.e.*, small misindexed areas) of the EBSD map. The grain size from EBSD maps can be obtained by ignoring this noise and subsequently fitting a log-normal curve to the rest of the grain size distribution graph. Because the noise occupies a significant fraction of the distribution, the frequency of grain sizes in the region without noise is underpredicted. This is adjusted in the following manner. First, a log-normal fit to the experimental grain size distribution is determined with similar width and ignoring the noise (Figure A6). Excluding the grain size region with noise, the area under the experimental curve is A and the area under the fit curve is B. An adjusted experimental grain size distribution is then constructed (Figure A7), with the frequency in each size class obtained by multiplying the frequency of the original experimental grain size distribution with (B/A), except for the smaller size classes affected by the noise. Subsequently, a log-normal fit to the adjusted experimental grain size distribution (Figure A7) is used to determine the ferrite grain size.

REFERENCES

1. M. Militzer: *Science*, 2002, vol. 298, pp. 975–76.
2. K.T. Park, S.Y. Han, B.D. Ahn, D.H. Shin, Y.K. Lee, and K.K. Um: *Scripta Mater.*, 2004, vol. 51, pp. 909–13.
3. T. Morimoto, I. Chikushi, R. Kurahashi, and J. Yanagimoto: *Proc. TMP 2004: 2nd Int. Conf. on Thermomechanical Processing of Steels*, Stahleisen Verlag GmbH, Düsseldorf, Germany, 2004, pp. 415–22.
4. R. Ueji, N. Tsuji, Y. Minamino, and Y. Koizumi: *Acta Mater.*, 2002, vol. 50, pp. 4177–89.
5. N. Tsuji, R. Ueji, Y. Minamino, and Y. Saito: *Scripta Mater.*, 2002, vol. 46, pp. 305–10.
6. L. Longfei, Y. Wangyue, and S. Zuqing: *Metall. Mater. Trans. A*, 2006, vol. 37A, pp. 609–19.
7. H. Dong and X. Sun: *Curr. Opin. Solid State Mater. Sci.*, 2005, vol. 9, pp. 269–76.
8. H. Beladi, G.L. Kelly, and P.D. Hodgson: *Metall. Mater. Trans. A*, 2007, vol. 38A, pp. 450–63.
9. H. Yada, Y. Matsumura, and K. Nakazima: U.S. Patent No. 4466842, Aug. 21, 1984.
10. Y. Matsumura and H. Yada: *Trans. ISIJ*, 1987, vol. 27, pp. 492–98.
11. H. Yada, Y. Matsumura, and T. Senuma: *Thermec '88-Int. Conf. on Physical Metallurgy of Thermomechanical Processing of Steels and Other Metals*, I. Tamura, ed., The Iron and Steel Institute of Japan, Tokyo, 1988, pp. 200–07.
12. C.M. Li, H. Yada, and H. Yamagata: *Scripta Mater.*, 1998, vol. 39, pp. 963–67.
13. M.R. Hickson, R.K. Gibbs, and P.D. Hodgson: *ISIJ Int.*, 1999, vol. 39, pp. 1176–80.
14. B. Eghbali and A. Abdollah-Zadeh: *Scripta Mater.*, 2006, vol. 54, pp. 1205–09.
15. J.Y. Cho, D.W. Suh, J.H. Kang, and H.C. Lee: in *Ultrafine-Grained Materials II*, Y.T. Zhu, T.G. Langdon, R.S. Mishra, S.L. Semiatin, M.J. Saran, and T.C. Lowe, eds., TMS, Warrendale, PA, 2002, pp. 259–65.
16. P.J. Hurley and P.D. Hodgson: *Mater. Sci. Eng., A*, 2001, vol. 302, pp. 206–14.
17. M.R. Hickson, P.J. Hurley, R.K. Gibbs, G.L. Kelly, and P.D. Hodgson: *Metall. Mater. Trans. A*, 2002, vol. 33A, pp. 1019–26.
18. P.D. Hodgson, M.R. Hickson, and R.K. Gibbs: *Scripta Mater.*, 1999, vol. 40, pp. 1179–84.
19. P.J. Hurley, B.C. Muddle, and P.D. Hodgson: *Metall. Mater. Trans. A*, 2001, vol. 32A, pp. 1507–17.
20. P.J. Hurley, P.D. Hodgson, and B.C. Muddle: *Scripta Mater.*, 1999, vol. 40, pp. 433–38.
21. H. Beladi, G.L. Kelly, A. Shokouhi, and P.D. Hodgson: *Mater. Sci. Eng., A*, 2004, vol. A367, pp. 152–61.
22. S.C. Hong, S.H. Lim, K.J. Lee, and K.S. Lee: in *Ultrafine-Grained Materials II*, Y.T. Zhu, T.G. Langdon, R.S. Mishra, S.L. Semiatin, M.J. Saran, and T.C. Lowe, eds., TMS, Warrendale, PA, 2002, pp. 267–74.
23. J.K. Choi, D.H. Seo, J.S. Lee, K.K. Um, and W.Y. Choo: *ISIJ Int.*, 2003, vol. 43, pp. 746–54.
24. S.C. Hong and K.S. Lee: *Mater. Sci. Eng., A*, 2002, vol. A323, pp. 148–59.
25. Z. Yang and R. Wang: *ISIJ Int.*, 2003, vol. 43, pp. 761–66.
26. H. Beladi, G.L. Kelly, A. Shokouhi, and P.D. Hodgson: *Mater. Sci. Eng., A*, 2004, vol. A371, pp. 343–52.
27. M. Militzer, R. Pandi, and E.B. Hawbolt: *Metall. Mater. Trans. A*, 1996, vol. 27A, pp. 1547–56.
28. D. Liu, F. Fazeli, and M. Militzer: *ISIJ Int.*, 2007, vol. 47, pp. 1789–98.
29. F.J. Humphreys: *J. Mater. Sci.*, 2001, vol. 36, pp. 3833–54.
30. R. Lottey and M. Militzer: in *Ultra-Fine Structured Steel*, E. Essadiqi and J. Thomson, eds., Metallurgical Society of CIM, Montreal, 2004, pp. 87–98.
31. T. Gladman and F.B. Pickering: *J. Iron Steel Inst.*, 1967, vol. 205, pp. 653–64.
32. "ASTM E384-99 Standard Test Method for Microindentation Hardness of Materials," *Annual Book of ASTM Standards*, ASTM, West Conshohocken, PA, 2000, vol. 3.01, pp. 437–60.
33. S.C. Hong, S.H. Lim, H.S. Hong, K.J. Lee, D.H. Shin, and K.S. Lee: *Mater. Sci. Eng., A*, 2003, vol. A355, pp. 241–48.
34. M. Mazinani and W.J. Poole: *Metall. Mater. Trans. A*, 2007, vol. 38A, pp. 328–39.
35. K. Mukherjee, S. Hazra, and M. Militzer: *Proc. SAE 2006 World Congr.*, SAE International, SP-2035, Detroit, MI, 2006, pp. 81–86.
36. K. Mukherjee, S. Hazra, P. Petkov, and M. Militzer: *Mater. Manuf. Processes*, 2007, vol. 22, pp. 511–15.
37. T. Morimoto, F. Yoshida, I. Chikushi, and J. Yanagimoto: *ISIJ Int.*, 2007, vol. 47, pp. 1475–84.
38. B. Hutchinson, L. Ryde, E. Lindh, and K. Tagashira: *Mater. Sci. Eng., A*, 1998, vol. A257, pp. 9–17.
39. T. Waterschoot, L. Kestens, and B.C. De Cooman: *Metall. Mater. Trans. A*, 2002, vol. 33A, pp. 1091–1102.
40. S. Zäfferer, J. Ohlert, and W. Bleck: *Acta Mater.*, 2004, vol. 52, pp. 2765–78.